SECTION III. TASK 3. COMPREHENSIVE MODEL DEVELOPMENT AND EVALUATION

Objectives

The objective of this task is to integrate advanced chemistry and physics submodels into a comprehensive two-dimensional model of entrained-flow reactors (PCGC-2) and to evaluate the model by comparing with data from well-documented experiments. Approaches for the comprehensive modeling of fixed-bed reactors will also be reviewed and evaluated and an initial framework for a comprehensive fixed-bed code will be employed after submission of a detailed test plan (Subtask 3.b).

Task Outline

This task is being performed in three subtasks. The first covers the full 60 months of the program and is devoted to the development of the entrained-bed code. The second subtask is for fixed-bed reactors and is divided into two parts. The first part (12 months) was devoted to reviewing the state-of-the-art in fixed-bed reactors. This led to the development of the research plan for fixed-bed reactors, which was approved. The code development is being done in the remaining 45 months of the program. The third subtask is to generalize the entrained-bed code to fuels other than dry pulverized coal and will be performed during the last 24 months of the program.

III.A. SUBTASK 3.A. - INTEGRATION OF ADVANCED SUBMODELS INTO ENTRAINED-FLOW CODE, WITH EVALUATION AND DOCUMENTATION

Senior Investigators - B. Scott Brewster and L. Douglas Smoot
Brigham Young University
Provo, UT 84602
(801) 378-6240 and 4326

Research Assistant - Susana K. Berrondo

Objectives

The objectives of this subtask are 1) to integrate the FG-DVC submodel into PCGC-2, 2) incorporate additional submodels and improvements developed under Task 2, 3) validate the improved code, 4) improve user-friendliness and robustness, and 5) document the code.

Accomplishments

Accomplishments during the 14th quarter on each of the above objectives are summarized below.

FG-DVC Submodel Integration

Work was temporarily suspended on the integration of the FG-DVC submodel awaiting a new submodel version to be produced by AFR. The new version will replace the time-consuming Monte Carlo approach with the faster two-sigma percolation theory (Hamblen and Serio, 1989a). In addition to being faster, the new version will be more stable numerically in PCGC-2.

Integration of Additional Submodels/Improvements

No other work on submodel integration was performed during the quarter.

Code Validation

Work continued on simulating the transparent wall reactor. Additional tomography data were received from AFR for the Rosebud coal flame and several improvements were made in the simulation, including grid refinement and incorporation of gas buoyancy and laminarization effects. A poster paper was

accepted for presentation at the 23rd International Symposium on Combustion to be held in Orleans, France on July 22-27.

Grid Refinement - The calculational grid was refined to concentrate the nodes in the flame zone and to locate nodes at the axial locations where radial data slices were provided by AFR. The latter modification was made to facilitate data comparison. A radial node spacing of 0.5 mm was used in the flame; outside the flame, the spacing was increased with radial distance by 10 percent for each adjacent cell. The axial node spacing was increased with axial distance by approximately 5 percent between adjacent cells, starting with a spacing of 2 mm at the screen.

Gas Buoyancy - Historically, body forces were neglected in the gas momentum equation in PCGC-2 because they are insignificant in most pulverized coal combustors, where the flow is highly turbulent. Neglecting gas body forces may be unacceptable in the transparent wall reactor, however, where the flow is laminar and non-isothermal. An option was therefore added for including a gravitational term in the axial-momentum equation. The gravitational term is included in the source term and assumes a negative value for up-fired systems and a positive value for down-fired systems.

Laminarization - The standard k-ε submodel used in PCGC-2 is not applicable to low-Reynolds-number flow. Previous reports describe the addition of a laminar-flow option to PCGC-2 to model the transparent wall reactor, but neither laminar nor turbulent predictions have provided adequate agreement with experimental data. Jones and Launder (1972, 1973) report a low-Reynolds-number modification to the k-ε model that Gillis (1989) incorporated in a 3-D fluid mechanics code. He reported negligible turbulence effects at low Reynolds numbers and consistency with the standard k-ε model at high Reynolds numbers. The laminar option in PCGC-2 was therefore modified to include the k-ε modification suggested by Jones and Launder. Basically, this modification consists of 1) including the viscous diffusion of k and ε, 2) allowing the model constants to depend on Reynolds number of turbulence, and 3) including additional terms to account for the non-isotropicity of the dissipation processes.

Simulation Results - Predicted particle trajectories are shown in Figure III.A-1 for five cases. The base case (Case 1) assumed an inlet coal stream diameter of 5 mm and one percent inlet gas turbulence intensity in the room air and preheated air streams. Laminarization and buoyancy effects were

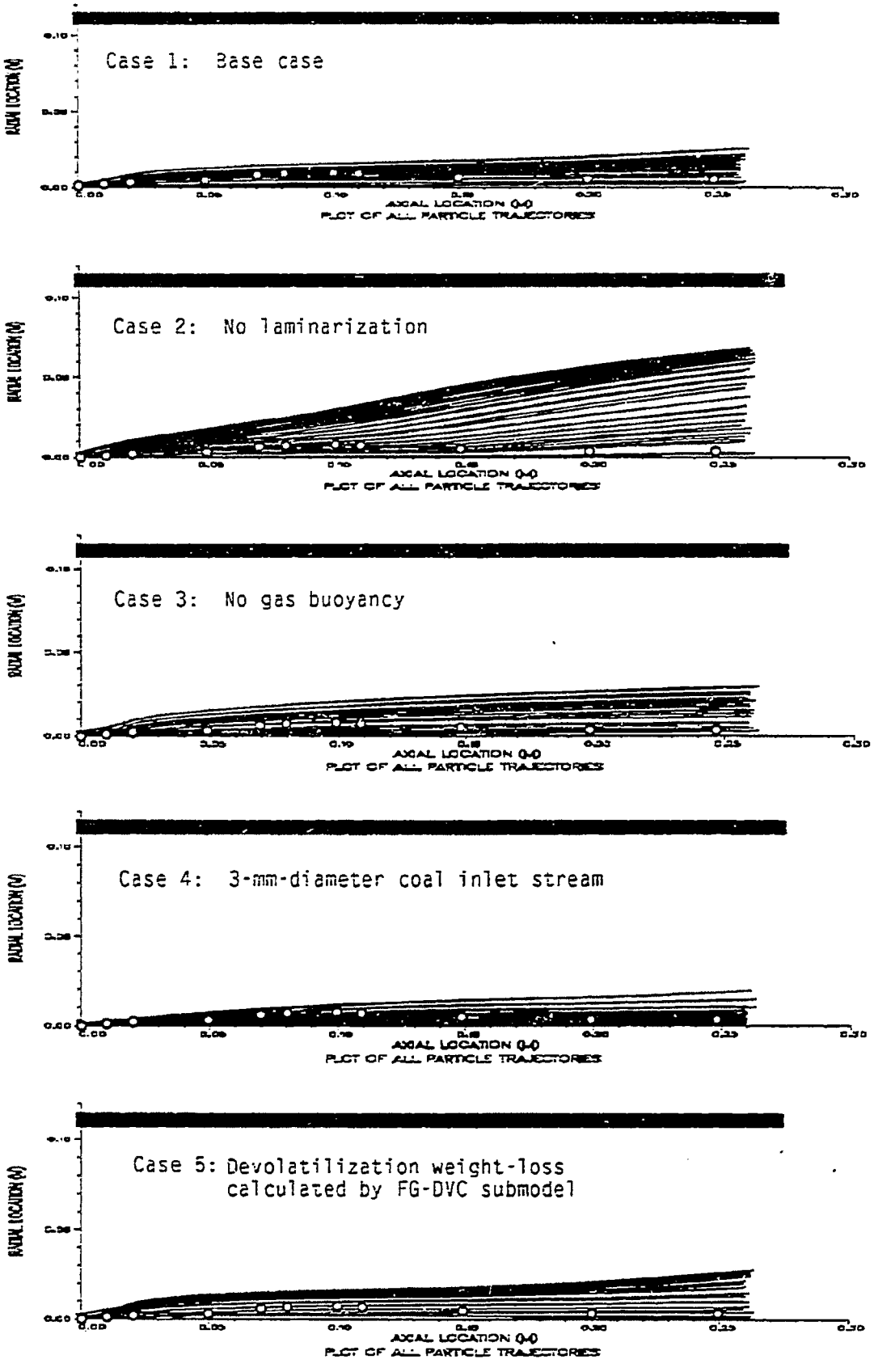

Figure III.A-1. Predicted particle trajectories and location of observed edge of coal stream (O) for combustion of Montana Rosebud subbituminous coal.

included. Devolatilization weight-loss was predicted by a single Arrhenius equation with $A = 7.5 \times 10^{14}$ s^{-1}, $E = 2.52 \times 10^{8}$ J/kmol, and a yield of 0.4 kg volatiles/kg raw coal. The four additional cases neglected laminarization (Case 2), neglected gas buoyancy (Case 3), assumed an inlet coal stream diameter of 3 mm (Case 4), and predicted devolatilization weight loss with the FG-DVC submodel (Case 5). The experimentally observed edge of the coal stream is also shown (Serio, 1989a) by the white circles. As shown, particle dispersion is somewhat overpredicted by the base case. Dispersion is extremely sensitive to neglecting laminarization, and is somewhat sensitive to neglecting gas buoyancy and changing the inlet coal stream diameter. It is quite insensitive to using the FG-DVC submodel instead of a single equation to predict devolatilization weight loss. Laminarization effects are definitely important in modeling this reactor.

Gas buoyancy increases the gas velocity at the centerline and induces an inward flow toward the centerline. The effects of this inward flow on the particle trajectories can be seen by comparing Cases 1 and 3 in Figure III.A-1. The effect of gas buoyancy on particle velocity is shown in Figure III.A-2. Predicted velocity for 60-μm particles at the centerline and outer edge of the coal stream are plotted as a function of axial distance. Velocity measurements determined from the length of particle streaks on photographs are also shown for comparison. In both cases (with and without buoyancy), the particles accelerate more rapidly in the predictions than the measurements indicate. Without buoyancy, the particles achieve a maximum velocity of 1.4 m/s, whereas velocities much higher than this have been measured. With buoyancy, the predicted velocities are higher than measured until the particles move far enough away from the centerline that the gas velocity starts decreasing. The observed diameter of the particle stream reaches a maximum of 2 cm at the ignition point (10 cm) and then converges back to a diameter of 1 cm. This convergence is presumably due to the inward flow induced by gas buoyancy, which overcomes the effects of particle dispersion due to turbulence. None of the cases shown in Figure III.A-1 predict this convergence of the particle stream after ignition. One explanation for this apparent discrepancy is that the particles dampen the gas turbulent fluctuations, thereby decreasing the turbulent particle dispersion. In the cases shown in Figure III.A-1, the effect of the particles on gas-phase turbulence was neglected. PCGC-2 is coded to include the effects of particle damping on gas turbulence according to the correlation of Melville and Bray (1979), and these effects are currently being investigated. If the predicted particle trajectories were to converge as experimentally observed, then both

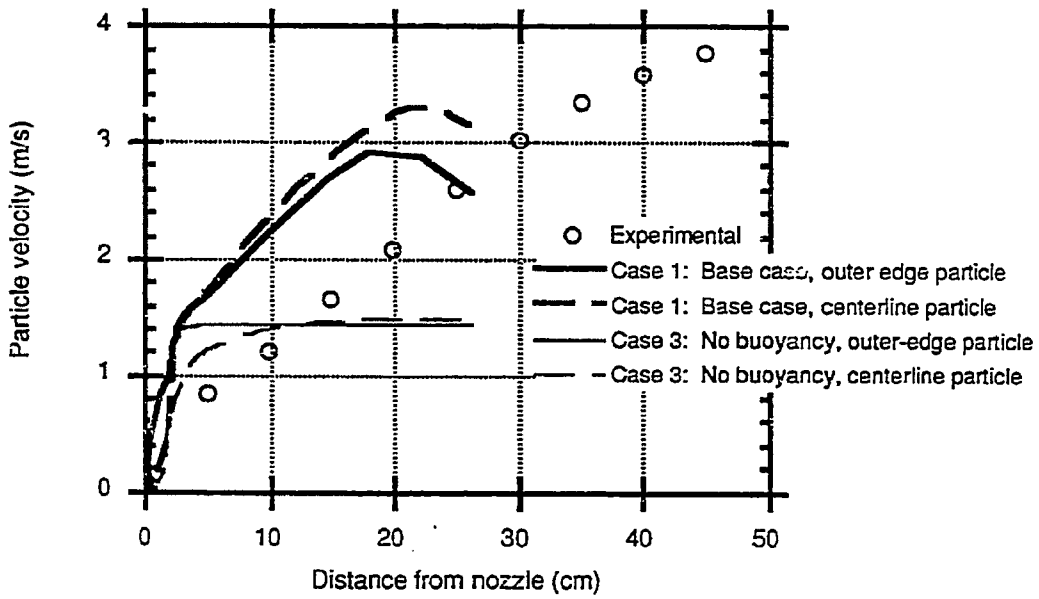

Figure III.A-2. Particle velocity determined from length of streaks in pnotographs compared with predicted particle velocity for 60μm particles starting at the centerline and at the outer edge of the coal stream, with and without gas buoyancy effects.

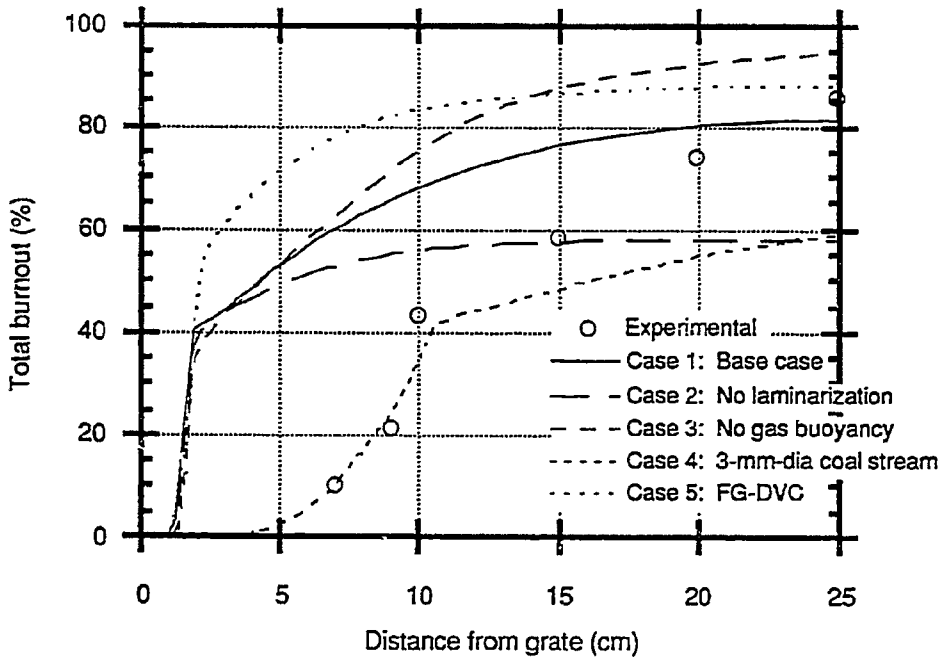

Figure III.A-3. Predicted and measured particle burnout showing effects of laminarization, gas buoyancy, particle stream inlet diameter, and devolatilization submodel.

particle dispersion and particle velocity would likely show better agreement with experimental observation.

The effects of particle dispersion and velocity on burnout are shown in Figure III.A-3. Burnout increases rapidly during devolatilization and more slowly during char oxidation. The ignition point is insensitive to all the parameter variations shown except coal stream diameter. When the diameter was changed from 5 mm to 3 mm, the ignition point changed from 2 cm to approximately 10 cm. The latter location is consistent with the experimental burnout data and with visual observation of the flame. The reason for the shift in ignition point is the increased velocity of the particles due to the smaller cross-sectional area of the stream. Burnout during char oxidation can be seen to be very sensitive to the parameter variations neglecting laminarization and gas buoyancy. This sensitivity is due to the sensitivity of particle dispersion and velocity to these variations. In Case 2, burnout is lower because the increased particle dispersion due to neglecting laminarization resulted in the outer particles being quenched in the room air before burnout was complete. In Case 3, burnout is higher because the lower gas velocity in the flame due to neglecting buoyancy resulted in increased particle residence time. It is interesting to note the absence of a sharp bend in the burnout curve for Case 5, due to the increased overlap and more gradual transition from devolatilization to char oxidation when the FG-DVC submodel was used.

Code Robustness and User-Friendliness

Energy Equation - Several minor improvements in the energy equation as well as additional insight into the energy coupling between the gas and solid phases resulted in successful convergence of a high-pressure, gasification case (Nichols, 1987). Historically, gasification cases have been difficult to converge, presumably because of steep temperature gradients in the flow field. The Nichols case is being considered for code validation. In addition to energy equation improvements, the robustness of the code was improved by solving the radiation and gas phase equations simultaneously for gaseous combustion cases. In particle combustion, the radiation submodel is decoupled and solved with the particles, after converging the gas field, since particle effects dominate the radiation.

Graphical User Interface - Work continued on a graphical user interface (GUI) for PCGC-2, based on the Sun windowing system, to make it easier for an

inexperienced user of PCGC-2 to set up and run cases on the Sun workstation. The GUI was extended to allow the user to specify the composition and temperature of inlet gas streams. A window for the primary stream is shown in Figure III.A-4. The window allows the user to toggle between boundary conditions of 0 and 1 for the inlet gas mixture fraction by clicking with the mouse on the circular arrows (↻) after the word REACTANTS. The appropriate set of reactant data then appear in the window, and the user can change the temperature or composition. The thermodynamic data file, containing data for all of the elements and chemical species in the simulation, is automatically generated from the data in the main data file and from a database which contains data for approximately 200 species.

Work was also initiated on applying two graphics programs, a pre- and post-processor developed under independent funding, to PCGC-2. The pre-processor generates a computational grid, and the post-processor displays code results. These two programs are based on the PHIGS graphics standard and are therefore portable to any workstation computer that supports PHIGS. During the last quarter, a conversion program was written to convert between the file format of the pre-processor and that of PCGC-2. An output subroutine was also developed for PCGC-2 that writes output files for the post-processor.

Code Documentation

Work continued under independent funding to update the PCGC-2 user's manual with general corrections. No documentation has been added to the manual to describe the new submodels and improvements that have been added to the code under this contract.

Plans

During the next quarter, the new FG-DVC submodel code version will be integrated into PCGC-2. The effect of particle damping of gas turbulence on particle dispersion in the TWR simulations will be investigated. Code predictions will be compared with tomography data from the TWR.

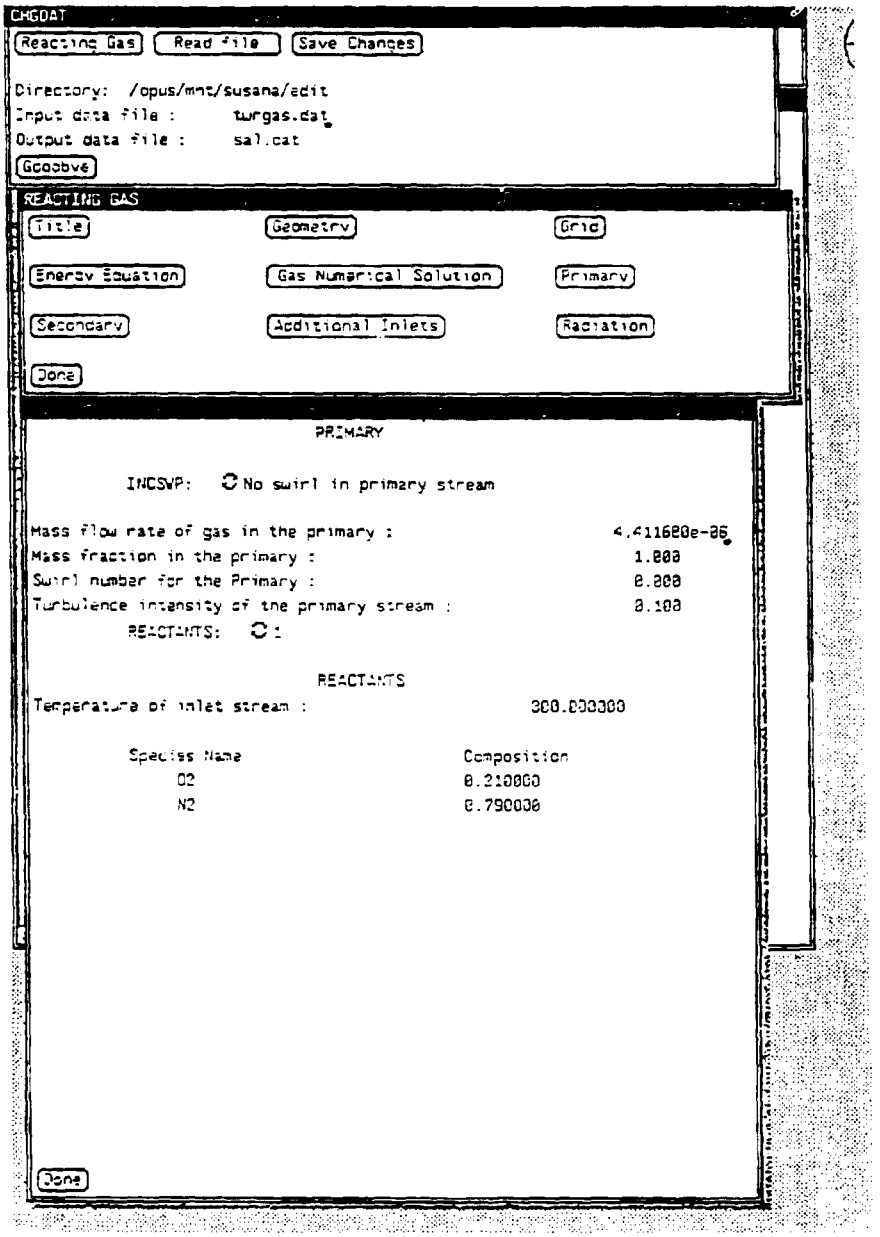

Figure III.A-4. Graphical user interface window on the Sun workstation which allows specification of temperature and composition of primary stream.

III.B. SUBTASK 3.B. - COMPREHENSIVE FIXED-BED MODELING REVIEW, DEVELOPMENT, EVALUATION, AND IMPLEMENTATION

Senior Investigators - Predrag T. Radulovic and L. Douglas Smoot
Brigham Young University
Provo, Utah 84602
(801) 378-3097 and (801) 378-4326

Graduate Research Assistant - Michael L. Hobbs

Objectives

The objectives of this subtask are: 1) to develop an advanced fixed-bed model incorporating the advanced submodels being developed under Task 2, particularly the large-particle submodel (Subtask 2.e.), and 2) to evaluate the advanced model.

Accomplishments

Overview

During the last quarter, work continued on reviewing, coding, and validation of submodels. Further work was performed on the well-mixed, partial-equilibrium submodel. The well-mixed, partial-equilibrium submodel provides an efficient and accurate initial estimate of the effluent composition and temperature for the one-dimensional model. The model includes detailed treatment of devolatilization, partial equilibrium of volatiles, treatment of a large number of gas phase species, and prediction of tar production with potential for recirculation of effluent products. Predictions have been compared to measured effluent temperatures and compositions from fixed-bed reactors. Quantitative agreement with experimental data has been obtained over a wide range of coal types. A paper describing the well-mixed model and model sensitivity was submitted to Combustion Science and Technology. This paper is included in **Appendix B.**

A presentation was given at the joint METC/AFR/BYU contract review meeting. AFR also met with BYU to discuss the interface between the fixed-bed code and the FG-DVC submodel. AFR verified BYU's understanding of the FG code. The final version of the fixed-bed code will retain the current implementation of the FG model with the tar predicted by the two-sigma

percolation DVC model. The interface between the two-sigma DVC model and the fixed-bed code with be through conservation of oligomer. The conservation of oligomer in both the solid and gas phases will be derived in terms of a system of first-order, ordinary differential equations based on percolation theory. The algorithm for solving this set of equations should be compatible with the LSODE solver used by the fixed-bed code.

Development of the one-dimensional, comprehensive, fixed-bed code (MBED-1D) is continuing. In order to enhance user-friendliness, the input file has been divided into parameters required for the well-mixed, partial-equilibrium submodel and those required for the 1-dimensional, fixed-bed code. Also, the code has been rewritten in a modular fashion with extensive comment statements. The well-mixed submodel has been improved to accommodate user-specified burnout. Also, a simple freeboard submodel has been written to accommodate heat loss in the void space above the coal bed.

Burnout

The influence of burnout on the dry, molar gas composition and temperature is shown in Figure III.B-1. Burnout is defined as the weight fraction of the organic matter in the raw coal that has reacted. The measured composition and input conditions are for Illinois #6 gasified at Westfield, Scotland. The input conditions are in the Appendix. The maximum temperature shown in Figure III.B-1b is a consequence of operating at fuel-rich conditions. In the fuel-rich gasifier, increasing burnout in the gasification/oxidation zone causes temperature to decrease. If burnout is small, the gas phase becomes oxygen-rich. Therefore, in the fuel-lean gasifier, increasing burnout causes the temperature of the oxidation zone to increase.

1-D Temperature and Composition Profiles

Modularization of the fixed-bed code resulted in better material and energy balances. To see the effect of changes, two validation cases were converged. The first case and input conditions were presented in Appendix B of the 13th Quarterly Report (Solomon et al., 1989d). This first case is gasification of Jetson high-volatile-B bituminous coal. Temperature and concentration profiles are given in Figure III.B-2. The gas phase concentration profile can be explained by following the solid temperature profile, starting at the bottom of the reactor. At the reactor bottom, the

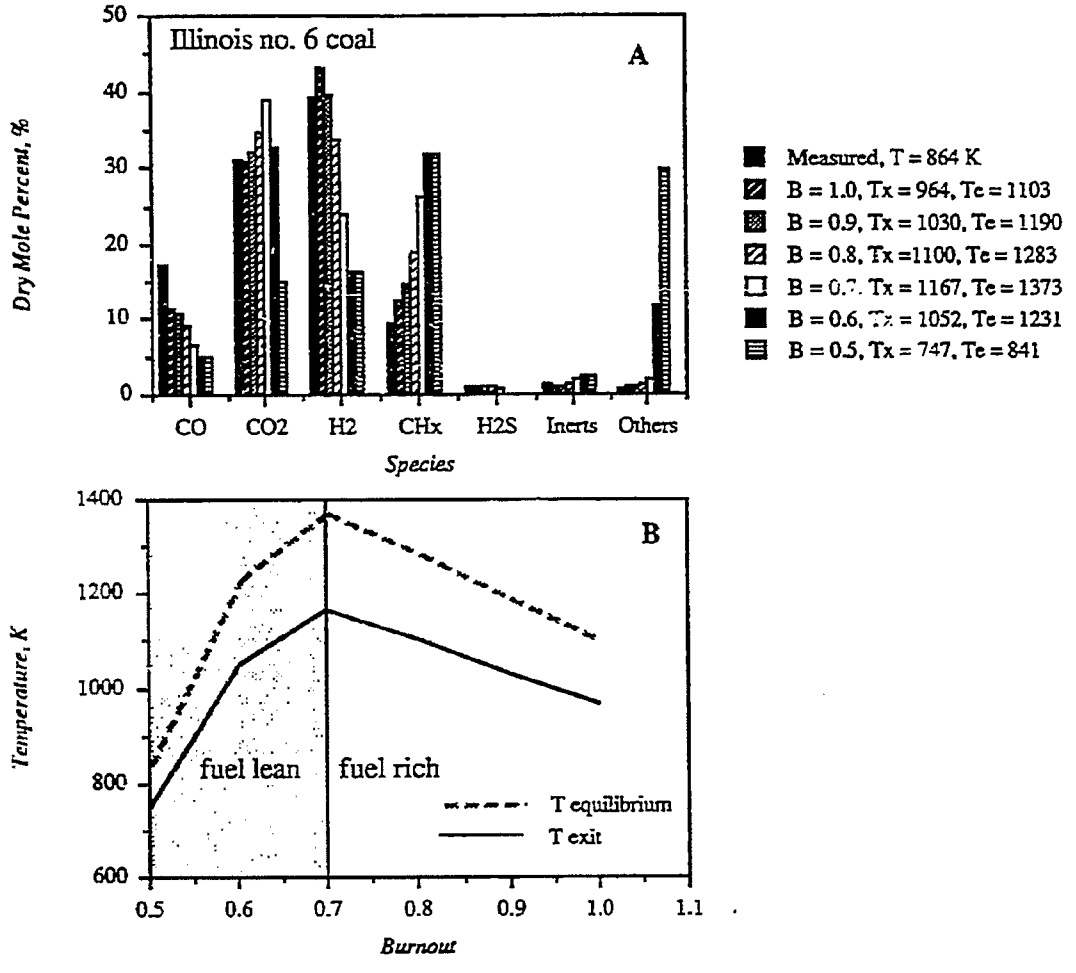

Figure III.B-1 Effluent gas composition, equilibrium temprature (Te), and exit (Tx) temperature, showing the influence of burnout (B) on the dry molar gas composition and temperature using the well-mixed, partial equilibrium model. Input parameters given in the Appendix.

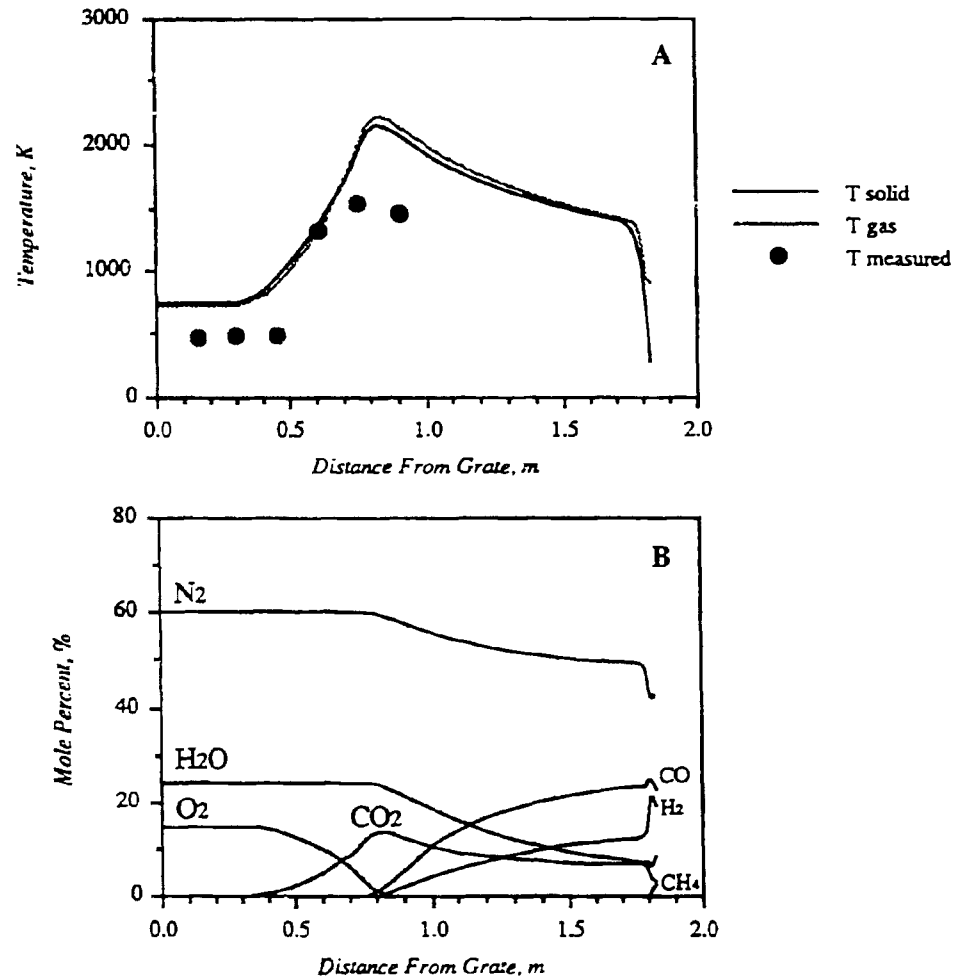

Figure III.B-2 A) Temperature and B) molar concentration profiles for gasification of Jetson high volatile B bituminous coal in at atmospheric pressure, air-fired, dry-ash gasifier. Input data are given in Solomon et al., 1990.

solid phase consists primarily of ash which exchanges energy with the countercurrent gas stream. As the solid increases in temperature, oxygen in the feed gas reacts heterogeneously with the solid carbon to form gaseous carbon monoxide and carbon dioxide. The carbon monoxide reacts homogeneously in the gas phase to form carbon dioxide. Steam also reacts with the solid carbon to form hydrogen and carbon monoxide. If oxygen is present in the gas phase, the hydrogen and carbon monoxide react homogeneously with oxygen to form steam and carbon monoxide. Thus, no depletion of steam is apparent until all gas-phase oxygen is depleted. Furthermore, only carbon dioxide is shown to increase in the presence of homogeneous oxygen. Although both steam and carbon dioxide react heterogeneously with the solid carbon, the gasification products from both reactions are oxidized to form carbon dioxide in the presence of oxygen.

The second case chosen for validation was the Westfield Illinois #6 gasification case used for the burnout sensitivity analysis shown in Figure III.B-1. Again the input parameters for this case can be found in the Appendix. The difference between the Wellman-Galusha case and the Westfield case is that the Wellman-Galusha is an air-fired, atmospheric gasifier, whereas the Lurgi gasifier used at Westfield is a high-pressure, oxygen-fired gasifier. The temperature and molar concentration profiles for the Westfield gasifier are given in Figure III.B-3. The shape of the temperature and concentration profiles are significantly different. The most obvious difference between the Wellman-Galusha case and the Westfield case is the absence of the carbon dioxide peak for the latter. Rather, the carbon dioxide profile produces a sigmoid or S-shaped curve. The shape of the carbon dioxide profile can be explained by the low temperature of the solid in the gasification section of the gasifier. The low temperature is a result of large quantities of steam in the feed gas stream. The temperature is low enough that the only significant heterogeneous reaction in this section of the gasifier is the steam gasification reaction. Gasification with carbon dioxide is essentially quenched due to low temperatures. With only hydrogen and carbon monoxide being produced in the gasification section, the hydrogen and carbon monoxide profiles should correspond. However, gas phase reactions such as the water-gas-shift reaction produces a slight increase in carbon dioxide concentration, creating a sigmoid profile rather than a peak as in the Wellman-Galusha case.

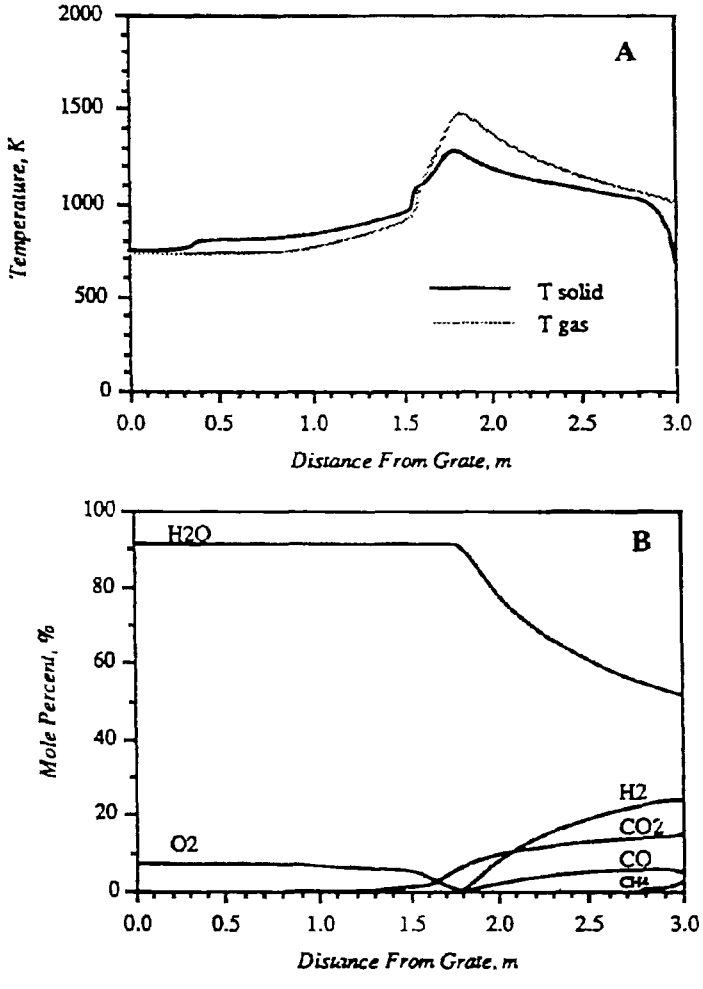

Figure III.B-3 A) Temperature and B) molar concentration profiles for gasification of Illinois #6 bituminous coal in a Lurgi, high-pressure, oxygen-fired, dry-ash gasifier. Input data can be found in the Appendix.

Plans

The development of the fixed-bed code will continue next quarter with emphasis on improving enthalpy calculations in the energy equations. A correlation for ash heat capacity based on ash constituents will be coded which takes into account the heat of melting and liquid ash heat capacity. The correlation was based on ash taken from a slagging, fixed-bed reactor (Mills and Rhine, 1989). Also, the two-sigma FG-DVC model will be implemented when available from AFR.

III.C. SUBTASK 3.C. - GENERALIZED FUELS FEEDSTOCK SUBMODEL

Senior Investigators - B. Scott Brewster and L. Douglas Smoot
Brigham Young University
Provo, UT 84602
(801) 378-6240 and 4326

Objective

The objective of this subtask is to extend PCGC-2 to accommodate generalized feedstocks consisting of both reacting and inert particles and gas in any inlet, including wall inlets.

Accomplishments

This subtask has not been initiated.

Plans

Initiate modification of PCGC-2 to allow injection of sorbent.